Electronic Supplementary Material (ESI) for Journal of Materials Chemistry A.
This journal is © The Royal Society of Chemistry 2021

Supporting Information

For

Contribution of BN-co-doped Reduced Graphene Oxide as a Catalyst Support on Activity of Iridium Oxide for Oxygen Evolution Reaction

Prerna Joshi[a], Rohit Yadav[a], Masanori Hara[a], Tetsunari Inoue[b], Yukihiro Motoyama[b], Masamichi Yoshimura[a]

[a]Surface Science Laboratory, [b]Catalytic Organic Chemistry Laboratory

Toyota Technological Institute, Nagoya, Japan

To whom correspondence should be addressed:
Prerna Joshi; Phone & Fax: 81-52-809-1852; Email: joshiprerna2011@toyota-ti.ac.jp; joshi.prerna2011@gmail.com

List of Figures:

Fig. S1	S-3
Fig. S2	S-3
Fig. S3	S-4
Fig. S4	S-4
Fig. S5	S-5
Fig. S6	S-6
Fig. S7	S-7
Fig. S8	S-8
Fig. S9	S-9
Fig. S10	S-10
Fig. S11	S-11
Fig. S12	S-12

List of Tables:

Table S1	S-2
Table S2	S-4
Table S3	S-5
Table S4	S-6
Table S5	S-7
Table S6	S-8
Table S7	S-9
Table S8	S-10
Table S9	S-11

Table S1 Catalysts with BN-bond structure reported in literature

Sample	***Application (As catalyst/support)***	***Electrolyte***	***η/mV at (j/ mA/cm^2)***	***Ref.***
pure IrO_x	OER (as catalyst)	1 M KOH	285 (10)	1
calcined-IrO_x	OER (as catalyst)	0.5 M H_2SO_4	260 (10)	2
IrO_x/L-BN	OER (as support)	1 M KOH	259 (10)	1
h-BN nanosheets supported on metal substrates (Cu and Au)	HER (as catalyst)	0.1 M $HClO_4$	−770 (20)	3
IrO_2-c-BN	OER (as support)	0.5 M H_2SO_4	400 (10)	This work
IrO_2-BN-rGO	OER (as support)	0.5 M H_2SO_4	300 (10)	This work

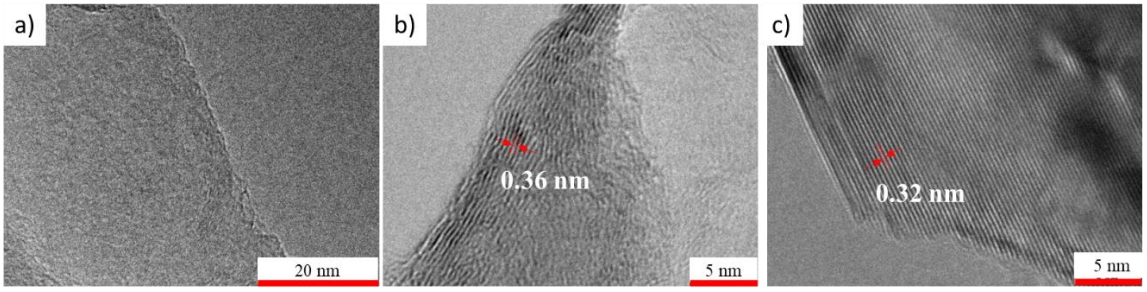

Fig. S1 TEM images of **a)** GO and **b)** rGO (lattice spacing: 0.36 ± 0.02 nm) and **c)** c-BN sheets (lattice spacing: 0.32 ± 0.03 nm)

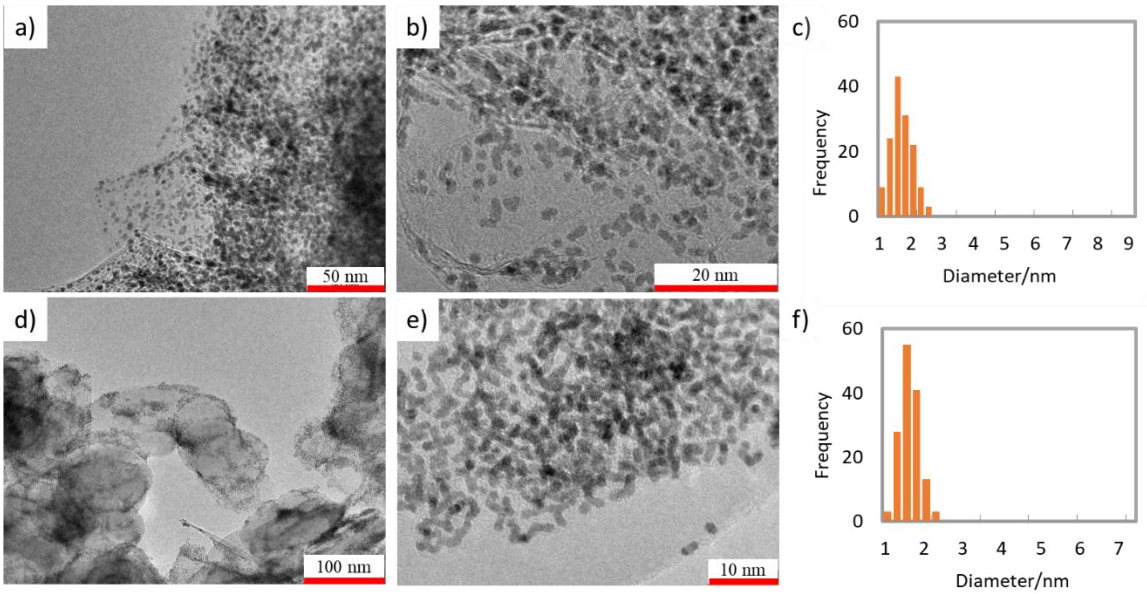

Fig. S2 TEM images of **a, b)** IrO_2-rGO, and **c)** its particle distribution.
TEM images of **d, e)** IrO_2-c-BN and **f)** its particle distribution.

For IrO_2-c-BN, although the particles were homogeneously distributed, the particles appeared both in spherical and non-spherical shapes. The average particle diameter calculated from the spherical nps was 1.6 ± 0.3 nm and the lattice spacing for IrO_2 nps was ca. 0.23 ± 0.01 nm.

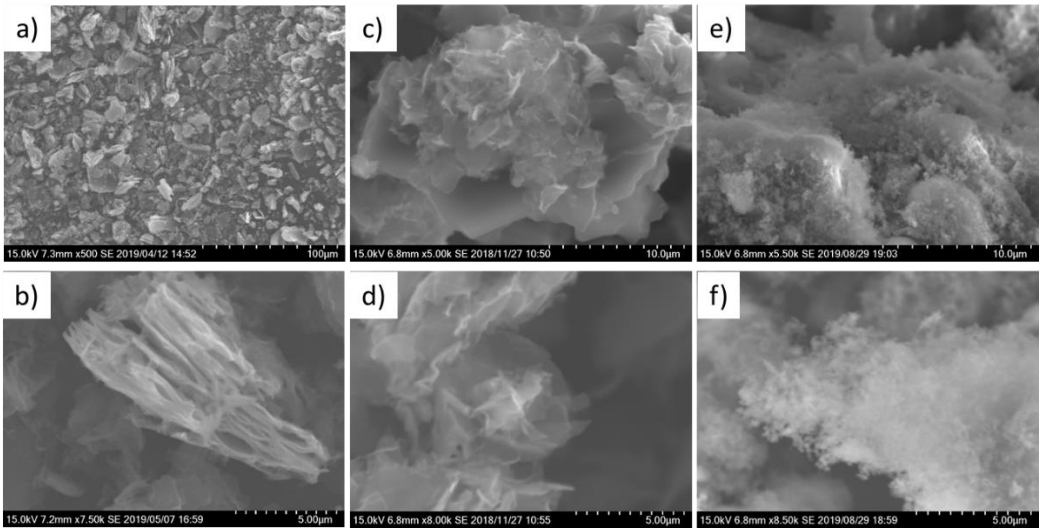

Fig. S3 SEM images of **a, b)** BN-rGO, **c, d)** rGO and **e, f)** c-BN

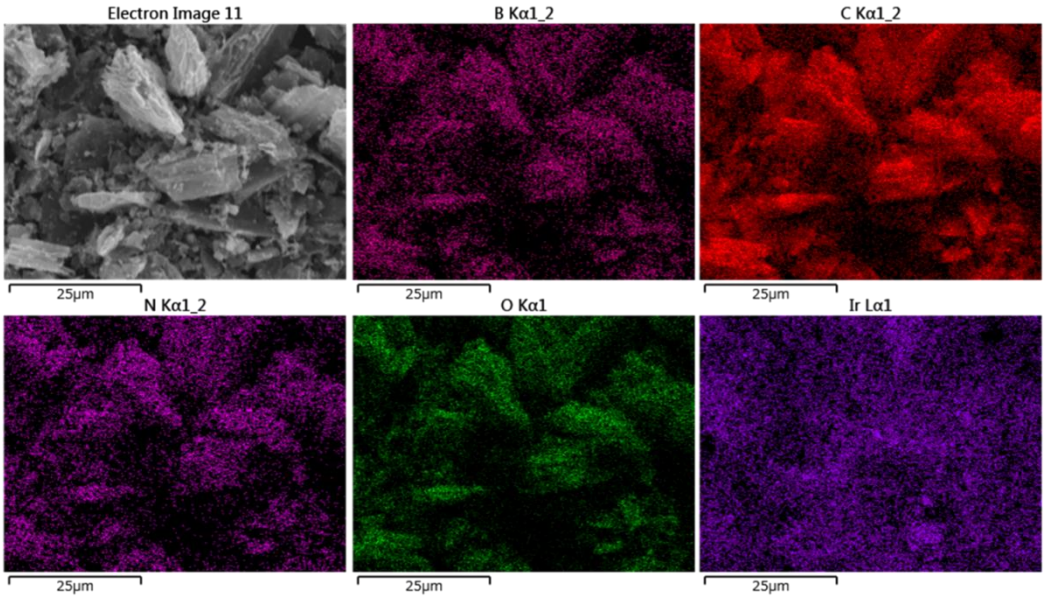

Fig. S4 EDX mapping of IrO_2-BN-rGO at 15 kV showing uniform distribution of all the constituent elements

Table S2 MP-AES results obtained for the designed catalysts

Catalyst	wt.% from EDX	wt.% from MP-AES
IrO_2-BN-rGO	12.1 ± 1.2	9.8
IrO_2-rGO	11.7 ± 1.2	11.2
IrO_2-c-BN	11.2 ± 1.1	11.8

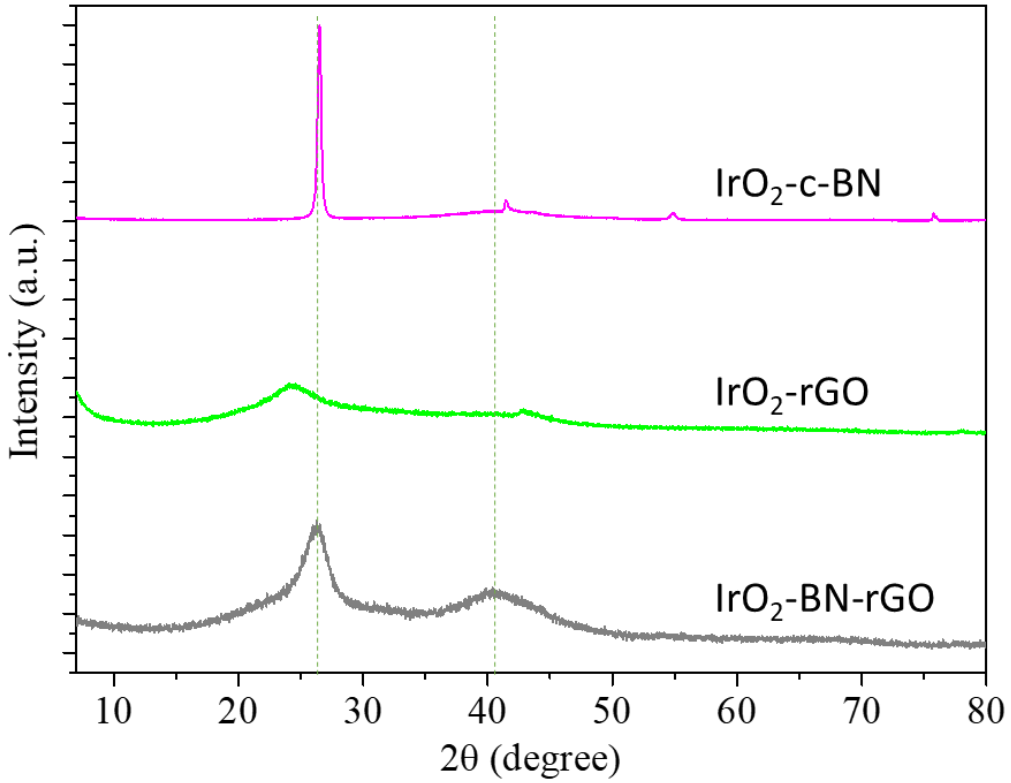

Fig. S5 XRD profiles of the catalysts, IrO_2-BN-rGO, IrO_2-rGO and IrO_2-c-BN

Table S3 Calculated *d*-spacing values for GO, rGO, BN-rGO and c-BN supports

Material	2θ	d spacing
GO	10.96	8.06
rGO	24.03	3.70
BN-rGO	26.34	3.38
c-BN	26.62	3.35

Similar to BN-rGO, a sharp peak at 2θ = 26.5°, referring to the (200) crystallographic plane of BN, was observed for c-BN exhibiting the highly crystalline and honeycomb-like hexagonal structure of c-BN comprising of B–N bonds. Additional weak peaks were observed at 2θ = 41.5°, 54.9° and 75.8°, corresponding to (100), (101) and (110) planes, respectively, which are consistent with the literature.[4] A small hump at 2θ =40.3° was also observed in IrO_2-c-BN after decoration with IrO_2 nps.

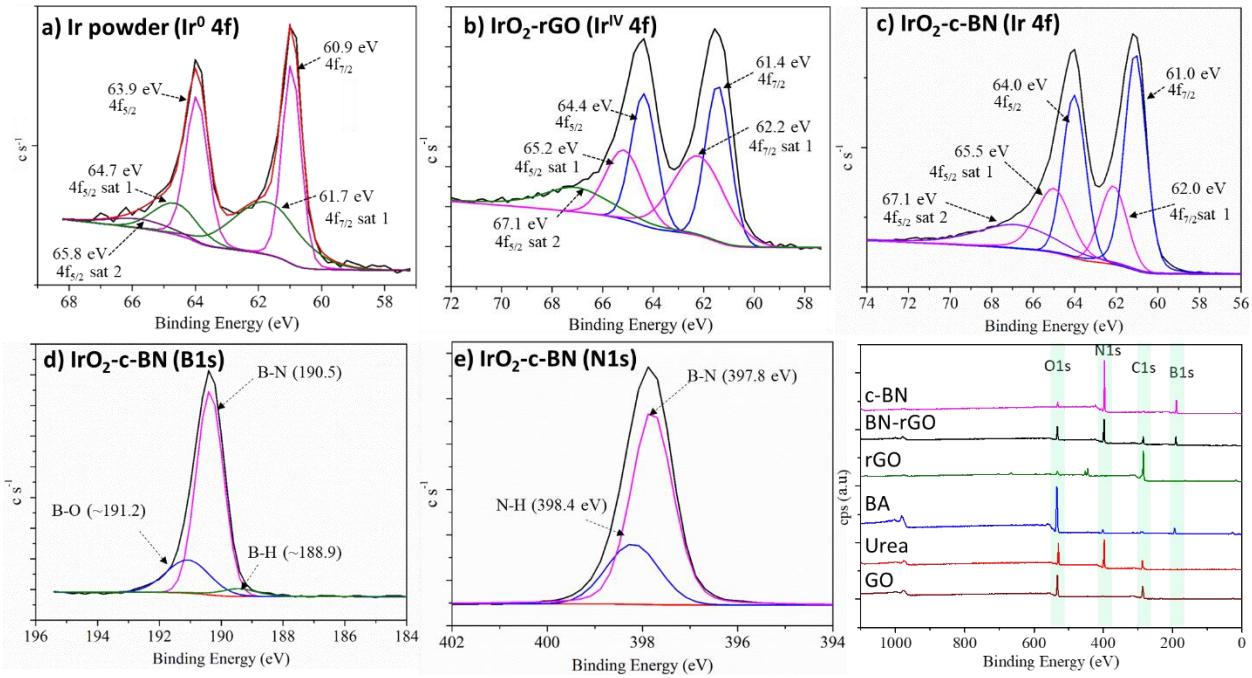

Fig. S6 Deconvoluted Ir 4f spectra of **a)** Ir powder, **b)** IrO_2-rGO, and **c)** IrO_2-c-BN. Deconvoluted **d)** B 1s and **e)** N 1s spectra for IrO_2-c-BN. **f**) Survey scan of all the precursors and supports

Table S4 Ir 4f peak positions and peak shift obtained from XPS spectra

Sample	**$4f_{7/2}$/ eV**	**$4f_{5/2}$/ eV**	**Peak Shift from Rutile type unsupported IrO_2/ eV**
Ir powder	60.9	63.9	0.9
IrO_2-rGO	61.4	64.4	0.4
IrO_2-B-rGO[5]	61.2	64.2	0.6
IrO_2-BN-rGO	61.1	64.1	0.7
IrO_2-c-BN	61.0	64.0	0.8
Rutile type unsupported IrO_2 [6]	61.8	64.8	0.0

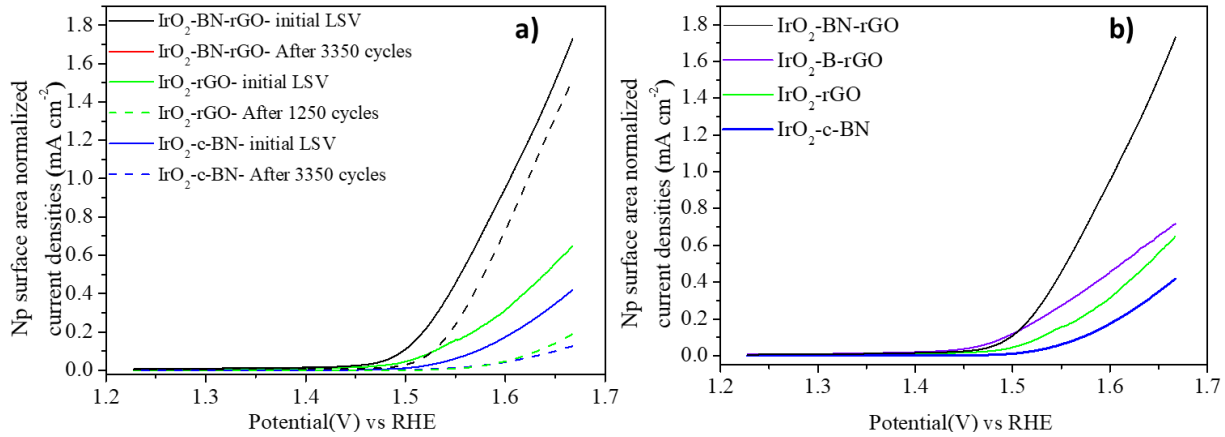

Fig. S7 Np surface area normalized LSV profiles for IrO_2 supported on different supports (obtained in 0.5 M H_2SO_4). The np surface area of IrO_2-BN-rGO, IrO_2-c-BN and IrO_2-rGO was calculated (from TEM) to be 36.56, 36.08 and 40.10 m^2 g_{Ir}^{-1}, respectively.

Table S5 List of OER activity of IrO_2 catalysts reported in recent literatures in 0.5 M H_2SO_4 with the value of overpotential measured at 10 $mAcm^{-2}$ at respective Ir loading

Catalyst	**Loading Ir ($mgcm^{-2}$)**	**Overpotential (mV) at 10 $mAcm^{-2}$**	**Reference**
Pt/IrO_2	0.300	330	7
Ir/Ti_4O_7	0.033	-	8
IrO_x-Ir	0.130	-	7
IrO_2	0.380	282	5
IrO_2-rGO	0.140	352	This work
IrO_2-N-rGO	0.140	-	9
IrO_2-B-rGO	0.140	283	5
IrO_2-BN-rGO	0.140	300	This work
IrO_2-c-BN	0.140	400	This work
Comm. IrO2 powder	0.287	430	5

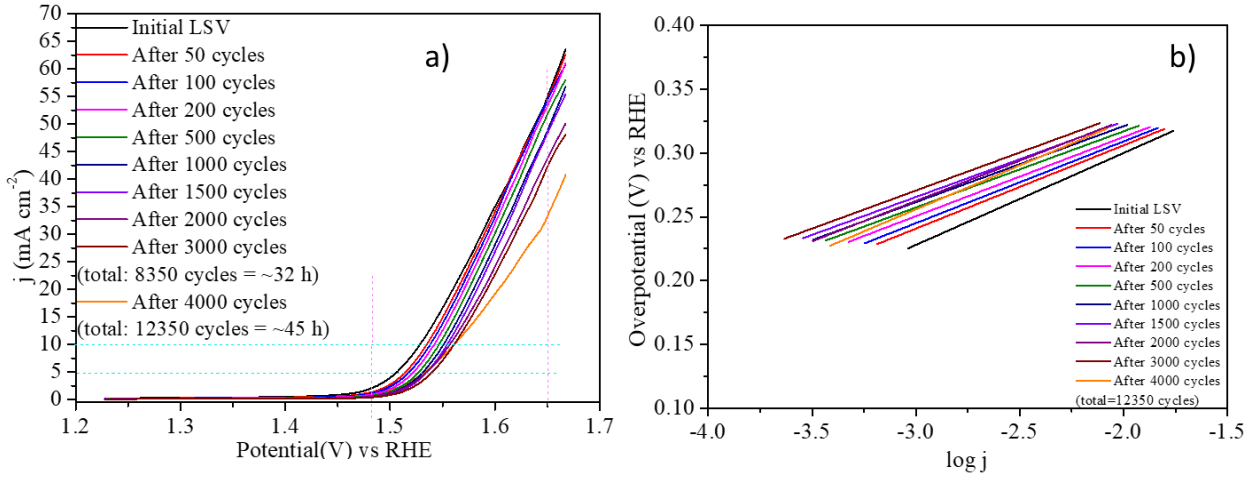

Fig. S8 a) Current density change of LSV on IrO_2-BN-rGO (12.1 wt.% Ir) during durability tests for 12350 cycles, and **b)** calculated Tafel slope of OER on IrO_2-BN-rGO estimated from LSV curve for all LSV profiles, measured in 0.5 M H_2SO_4 solution between 1.20 to 1.65 V vs RHE

Table S6 Calculated current densities (j / mAcm^{-2}) at 1.48 and 1.65 V vs RHE, overpotential (η / V) at 5 and 10 mAcm^{-2}, onset potential (V), Tafel slope (mV dec^{-1}) from LSV curve and calculated mass activities (A g_{Ir}^{-1}) with increasing no. of cycles for IrO_2-BN-rGO.
*All the errors in Tafel slopes are in the range of 10^{-4}.

No of ADT cycles (total cycles)	j (mAcm^{-2}) at 1.48 V	j (mA cm^{-2}) at 1.65 V	η (V) at 5 mAcm^{-2}	η (V) at 10 mAcm^{-2}	Onset potential (V)	Tafel slope (mV dec^{-1})	Mass activity (A g_{Ir}^{-1})
1 (0)	1.92	55.02	0.28	0.30	1.48	72.1 ± 0.02	13.82
50 (50)	1.25	54.37	0.28	0.30	1.49	65.2 ± 0.02	9.13
100 (150)	1.09	54.37	0.28	0.31	1.50	64.0 ± 0.01	7.76
200 (350)	0.89	53.23	0.29	0.31	1.50	62.0 ± 0.01	6.38
500 (850)	0.67	51.75	0.30	0.32	1.51	59.7 ± 0.01	5.51
1000 (1850)	0.57	48.89	0.30	0.32	1.51	59.5 ± 0.02	4.80
1500 (3350)	0.48	48.32	0.30	0.32	1.51	59.3 ± 0.01	4.11
2000 (5350)	0.57	43.83	0.31	0.33	1.51	63.2 ± 0.02	3.50
3000 (8350)	0.40	42.28	0.31	0.33	1.52	59.6 ± 0.02	4.14
4000 (12350)	0.77	33.29	0.30	0.33	1.51	68.8 ± 0.01	2.88

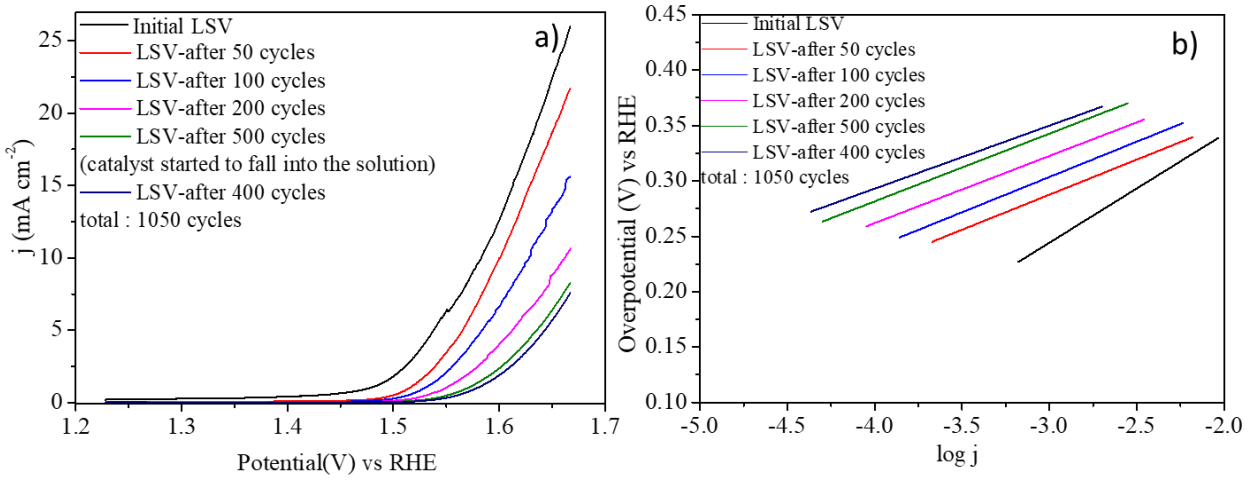

Fig. S9 a) Current density change of LSV on IrO_2-rGO (11.7 wt.% Ir) during durability tests for 1250 cycles, and **b)** calculated Tafel slope of OER on IrO_2-rGO estimated from LSV curve for all LSV profiles, measured in 0.5 M H_2SO_4 solution between 1.20 to 1.65 V vs RHE

Table S7 Calculated current densities (j / mAcm^{-2}) at 1.48 and 1.65 V vs RHE, overpotential (η / V) at 5 mAcm^{-2}, onset potential (V), Tafel slope (mV dec^{-1}) from LSV curve and ca. mass activities (A g_{Ir}^{-1}) with increasing no. of cycles for IrO_2- rGO.

No of ADT cycles (total cycles)	***j*** **(mAcm^{-2}) at 1.48 V**	***j*** **(mA cm^{-2}) at 1.65 V**	**η (V) at 5 mAcm^{-2}**	**η (V) at 10 mAcm^{-2}**	**Onset potential (V)**	**Tafel slope (mV dec^{-1})**	**Mass activity (A g_{Ir}^{-1})**
1 (0)	1.05	22.29	0.308	0.352	1.47	98.0 ± 0.0005	7.52
50 (50)	0.23	18.61	0.335	0.369	1.50	63.3 ± 0.0004	1.66
100 (150)	0.13	13.19	0.353	0.398	1.51	63.7 ± 0.0005	0.92
200 (350)	0.06	8.750	0.381	0.432	1.54	60.7 ± 0.0004	0.45
500 (850)	0.04	6.273	0.405	0.450*	1.56	61.1 ± 0.0003	0.28
400 (1250)	0.03	5.568	0.410	0.460*	1.57	56.9 ± 0.0003	0.18
*after extrapolation							

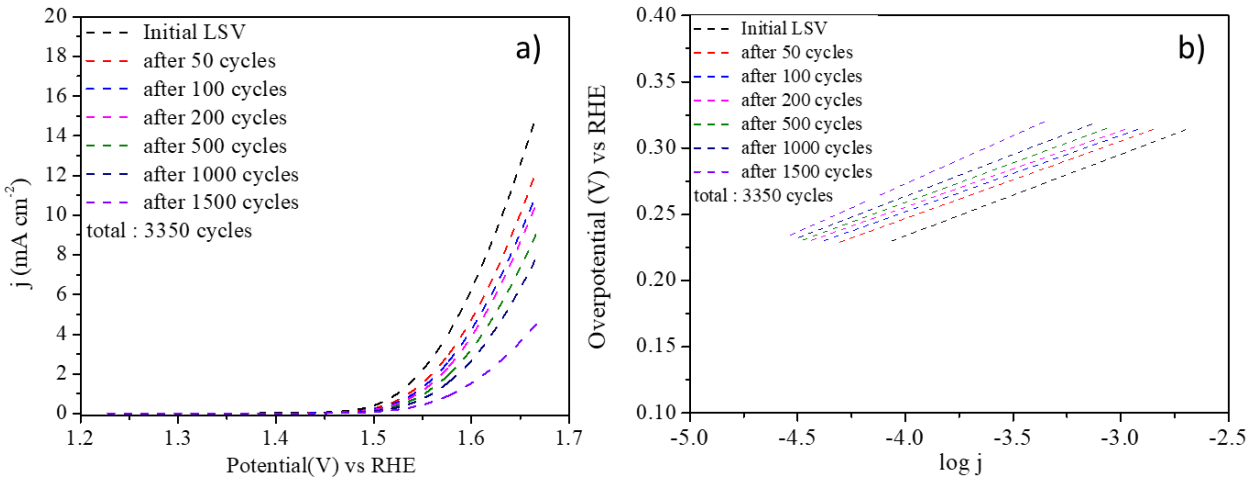

Fig. S10 a) Current density change of LSV on IrO_2-c-BN (11.2 wt.% Ir) during durability tests for 3350 cycles, and **b)** calculated Tafel slope of OER on IrO_2-BN-rGO estimated from LSV curve for all LSV profiles, measured in 0.5 M H_2SO_4 solution between 1.20 to 1.65 V vs RHE

Table S8 Calculated current densities (j / mAcm^{-2}) at 1.48 and 1.65 V vs RHE, overpotential (η / V) at 5 and 10 mAcm^{-2}, onset potential (V), Tafel slope (mV dec^{-1}) from LSV curve and ca. mass activities (A g_{Ir}^{-1}) with increasing no. of cycles for IrO_2-c-BN.
*All the errors in Tafel slopes are in the range of 10^{-4}.

No of ADT cycles (total cycles)	***j*** **(mAcm^{-2}) at 1.48 V**	***j*** **(mA cm^{-2}) at 1.65 V**	**η (V) at 5 mAcm^{-2}**	**η (V) at 10 mAcm^{-2}**	**Onset potential (V)**	**Tafel slope (mV dec^{-1})**	**Mass activity (A g_{Ir}^{-1})**
1 (0)	0.18	12.53	0.36	0.40	1.50	61.0 ± 0.01	1.24
50 (50)	0.11	10.05	0.37	0.41	1.51	58.4 ± 0.02	0.78
100 (150)	0.09	9.09	0.38	0.43	1.52	57.7 ± 0.01	0.62
200 (350)	0.08	8.64	0.38	0.43	1.52	57.6 ± 0.03	0.56
500 (850)	0.07	7.35	0.39	0.44*	1.52	59.7 ± 0.01	0.47
1000 (1850)	0.06	6.34	0.40	0.46*	1.53	62.9 ± 0.01	0.40
1500 (3350)	0.05	3.63	0.44*	0.53*	1.55	72.6 ± 0.02	0.31
*after extrapolation							

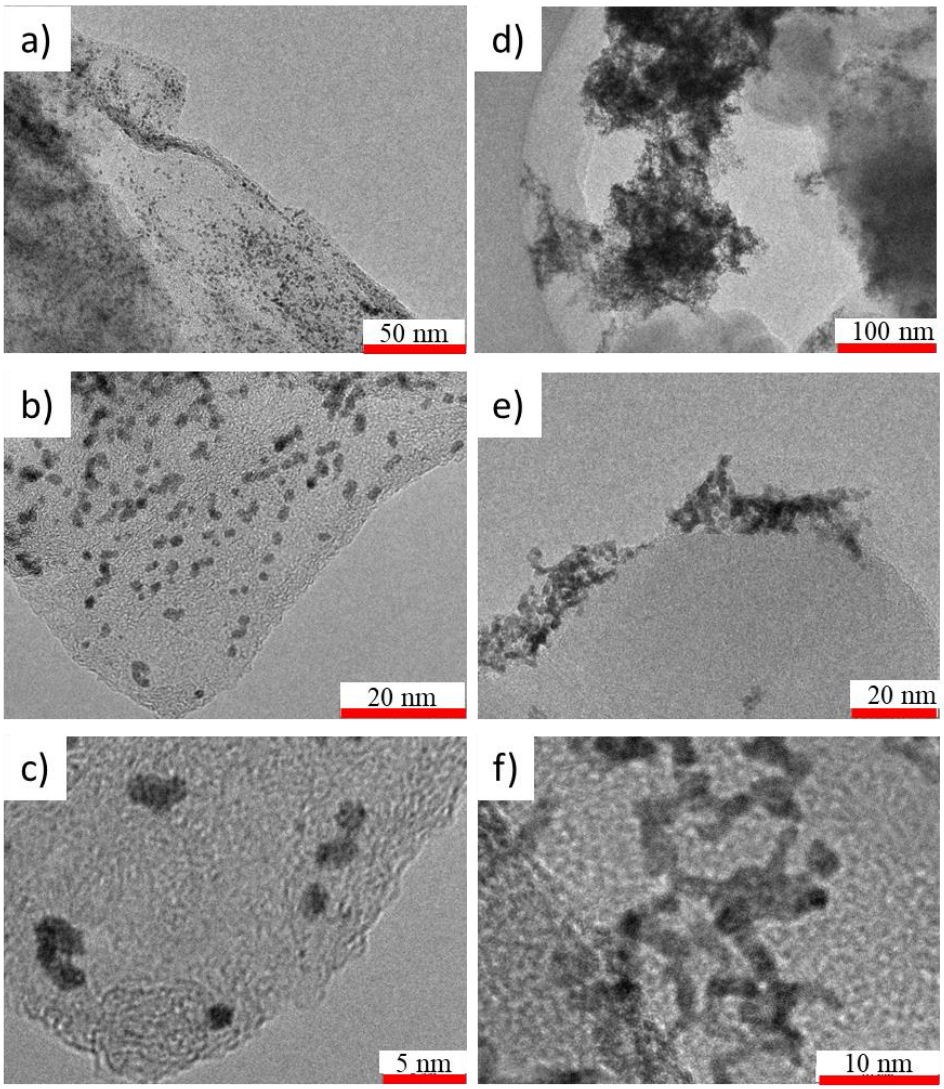

Fig. S11 TEM images of **a, b, c)** IrO_2-rGO and **d, e, f)** IrO_2-c-BN sheets after ADT indicating degradation of IrO_2 nps via aggregation and shape distortion

Table S9 Elemental composition of IrO_2-BN-rGO estimated via XPS before and after ADT

Elements	**Element Composition (at. %)**	
	Before ADT	**After ADT**
B 1s	34.37	3.07
C 1s	2.99	8.43
N 1s	29.19	8.32
O 1s	27.41	48.73
Si 2p	-	28.05
Ir 4f	5.62	3.41

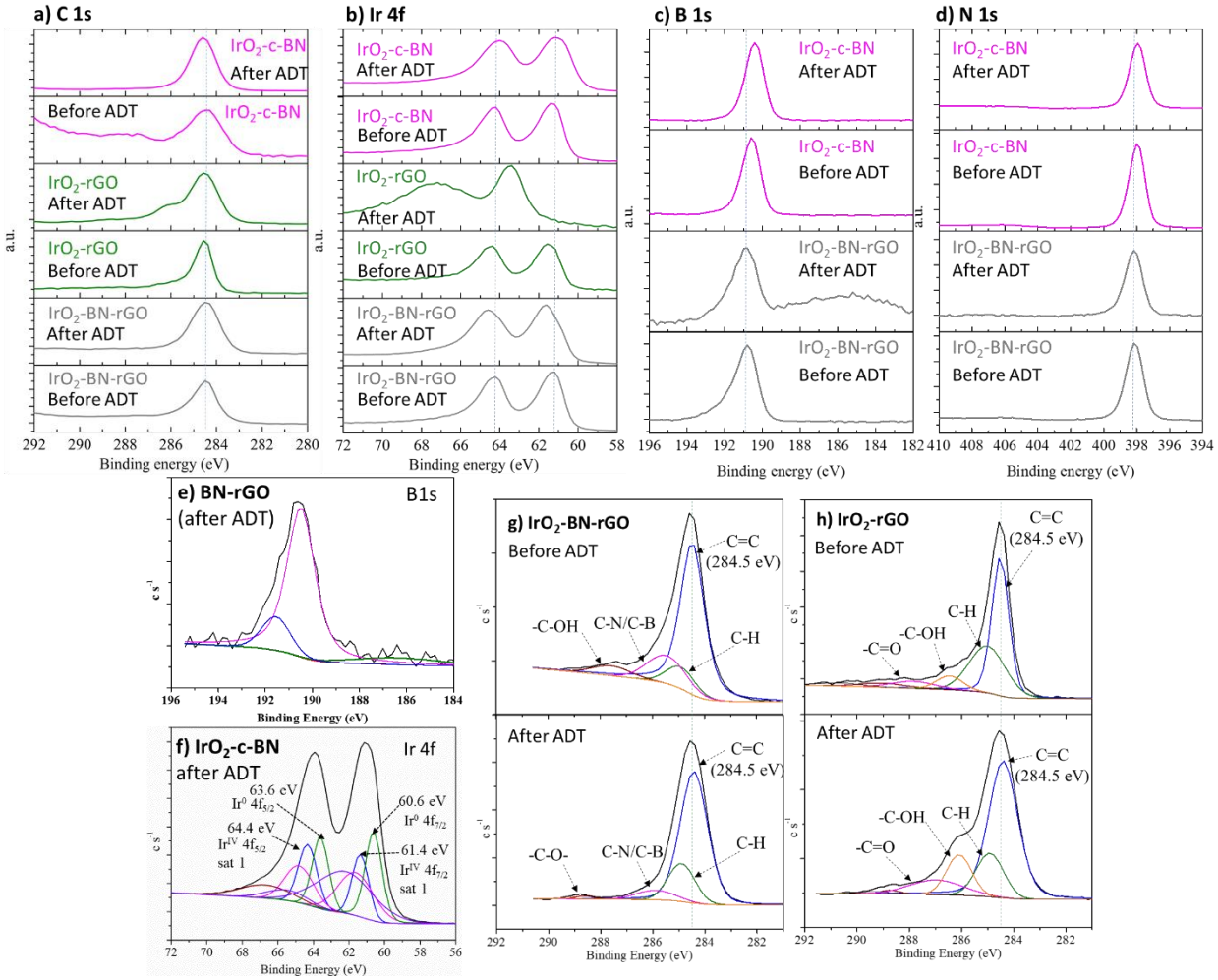

Fig. S12 Comparison of XPS spectra of **(a)** C 1s and **(b)** Ir 4f **(c)** B 1s, and **(d)** N 1s for IrO_2-BN-rGO, IrO_2-rGO and IrO_2-c-BN before and after ADT; **e)** B 1s deconvolution of BN-rGO support after ADT; **(f)** Ir 4f deconvolution of IrO_2-c-BN after ADT. C 1s deconvolution of **g)** IrO_2-BN-rGO and **h)** IrO_2-c-BN before and after ADT

The Ir 4f deconvolution of IrO_2-c-BN in **Figure S12f** displayed higher metallic character (high peak intensity and peak area for Ir^0 4f peaks) compared to IrO_2-BN-rGO (**Figure 8h**).

References:

1 H. Liu, X. H. Zhang, Y. X. Li, X. Li, C. K. Dong, D. Y. Wu, C. C. Tang, S. L. Chou, F. Fang and X. W. Du, *Adv. Energy Mater.*, 2020, **10**, 1–7.

2 G. C. da Silva, N. Perini and E. A. Ticianelli, *Appl. Catal. B Environ.*, 2017, 218, 287-297.

3 D. Q. Liu, B. Tao, H. C. Ruan, C. L. Bentley and P. R. Unwin, *Chem. Commun.*, 2019, **55**, 628-631.

4 N. Kostoglou, J. Lukovic, B. Babic, B. Matovic, D. Photiou, G. Constantinides, K. Polychronopoulou, V. Ryzhkov, B. Grossmann, C. Mitterer and C. Rebholz, *Mater. Des.*, 2016, **110**, 540–548.

5 P. Joshi, H. H. Huang, R. Yadav, M. Hara and M. Yoshimura, *Catal. Sci. Technol.*, 2020,**10**, 6599-6610.

6 V. Pfeifer, T. E. Jones, J. J. Velasco Vélez, C. Massué, M. T. Greiner, R. Arrigo, D. Teschner, F. Girgsdies, M. Scherzer, J. Allan, M. Hashagen, G. Weinberg, S. Piccinin, M. Hävecker, A. Knop-Gericke and R. Schlögl, *Phys. Chem. Chem. Phys.*, 2016,**18**, 2292-2296.

7 G. C. Da Silva, M. R. Fernandes and E. A. Ticianelli, *ACS Catal.*, 2018, **8**, 3, 2081–2092.

8 P. Lettenmeier, L. Wang, U. Golla-Schindler, P. Gazdzicki, N. A. Cañas, M. Handl, R. Hiesgen, S. S. Hosseiny, A. S. Gago and K. A. Friedrich, *Angew. Chemie - Int. Ed.*, 2016, **55**, 2, 742-746.

9 M. Hara, R. Badam, G. J. Wang, H.-H. Huang and M. Yoshimura, *ECS Trans.*, 2018, **85**, 27–35.